scientific reports

Check for updates

OPEN

Study of acute lethality, teratogenesis, and metabolomic changes of *N*-(2′-hydroxyphenyl)-2-propylpentanamide (HO-AAVPA) on *Artemia franciscana*

Cynthia Fernández-Pomares[1]✉, Alan Rubén Estrada-Pérez[1], Humberto L. Mendoza-Figueroa[1], Juan Benjamín García-Vázquez[1], Martha C. Rosales-Hernández[2] & José Correa-Basurto[1]✉

The brine shrimp lethality test (*Artemia* spp.) is a classical model for assessing the toxicity of bioactive compounds. This study evaluated the toxicity and metabolomic changes induced by *N*-(2′- hydroxyphenyl)-2-propylpentanamide (HO-AAVPA), a derivative of valproic acid (VPA), in *Artemia franciscana* larvae using untargeted metabolomics through liquid chromatography–mass spectrometry (LC-MS/MS). The lethal concentration 50 (LC_{50}) was determined by acute toxicity tests at 24 and 48 h, and teratogenic effects were assessed by measuring the larvae body length. Larval metabolomic changes were examined following 24- and 48-hour exposures to sublethal concentrations of HO-AAVPA (LC_1 = 0.04 mM, LC_{10} = 0.2 mM) and VPA (LC_1 = 1.79 mM, LC_{10} = 8.95 mM). After 48 h, HO-AAVPA had an LC_{50} of 0.32 mM, while VPA had 18.7 mM. VPA induced teratogenic effects at 9.6 mM; in contrast, HO-AAVPA only significantly affected the body length at 0.56 mM. Metabolomic analysis revealed that sublethal concentrations of HO-AAVPA affected the sphingolipid and glycerophospholipid metabolism, while VPA impacted alanine, aspartate, and glutamate metabolism. These findings suggest HO-AAVPA has high toxicity, but lower teratogenicity compared to VPA. In conclusion, the present study indicates that alterations in lipid and amino acid metabolism could be critical points in the mode of action of these compounds in *A. franciscana*.

Keywords Acute toxicity text, LC-MS/MS, Valproic acid, Histone deacetylase inhibitors, Untargeted metabolomics.

Animal models have played a central role in discovering and developing new drugs during pre-clinical studies[1]. Unlike in vitro systems, animal models allow for a deep understanding of the effects of new molecules with therapeutic potential in a complete biological system. This provides a broader picture of the efficacy, action mechanisms, and toxic effects of drugs before their application in clinical trials. However, ethical concerns related to using animals in experimentation, high maintenance cost, and the prolonged development time limit the capacity of these models[2].

Less complex organisms have been used as alternatives to mammals in drug screening tests. *Artemia* spp., a crustacean from the Branchiopoda class, has been used as an ecotoxicological model due to its sensitivity to environmental stressors[3]. This crustacean is characterized by its short life cycle, fast development, easy manipulation, and availability[4], making it an excellent biological model for testing the effectiveness of new synthetic, semisynthetic compounds, and natural products in high quantities, with low costs, and expedited identification of the most promising compounds[5].

In ecotoxicology, researchers have suggested using the *Artemia* model to evaluate the impact of environmental pollutants on metabolomic studies[6,7]. This approach aims to determine the mechanisms of toxicological action

[1]Laboratorio de Diseño y Desarrollo de Nuevos Fármacos e Innovación Biotecnológica, Escuela Superior de Medicina, Instituto Politécnico Nacional, Plan de San Luis y Díaz Mirón, 11340 Mexico City, Mexico. [2]Laboratorio de Biofísica y Biocatálisis, Sección de Estudios de Posgrado e Investigación, Escuela Superior de Medicina, Instituto Politécnico Nacional, Mexico City, Mexico. ✉email: cyfernandez@uv.mx; corrjose@gmail.com

and potential exposure biomarkers[8]. However, pharmacology applications of brine shrimp are mostly limited to acute lethality assays for bioactive compounds identification and, less frequently, for teratogenicity[9,10] and neurotoxicity assessments[11,12].

Metabolomic studies applied in the *Artemia* spp. can enhance the toxicological evaluation of new molecules by understanding the metabolic changes and mode of action that cause the effects of potential drugs[13]. This could contribute to an understanding of the impact of new compounds in initial studies before they are evaluated in more complex animals, improving experimental planning in mammals and potentially reducing the number of animals required for starting an evaluation in an in vivo model[2].

Under this premise, we investigate the impact of *N*-(2-hydroxyphenyl)-2-propylpentanamide (HO-AAVPA) on acute toxicity and its metabolomic deregulation on *Artemia* model previously used for screening the *Sargassum* toxicities by our work group[14]. HO-AAVPA was designed by in silico tools as a hybrid molecule comprising valproic acid (VPA) and a hydroxy-benzylamide fragment, which serves as a non-hydroxamic zinc-binding group[15]. Like its precursors, HO-AAVPA is a histone deacetylase inhibitor (HDACi) that regulates breast cancer cell growth, proliferation, and cell death[15]. HO-AAVPA has higher bioavailability[16] and lower toxicity than VPA in rodent models[17,18]. Metabolomic studies of HO-AAVPA have been tested in vitro using MDA-MB-231 and MCF-7 breast cancer cells, showing lipid deregulation[19].

This study aims to evaluate the acute toxicity and teratogenic effects of VPA and HO-AAVPA on *A. franciscana* larvae. We also studied the deregulated metabolites under an untargeted LC-MS/MS metabolomics approach. This work seeks to expand the brine shrimp lethality model to achieve an integral overview of the pharmacological action of new compounds.

Materials and methods

Acute lethal and teratogenicity assays

Artemia franciscana hatching

The hatching of *A. franciscana* cysts (White Mountain, Great Salt Lake Utah, USA) followed the protocol provided by the *Aquarium del Puerto de Veracruz* (formerly known as *Acuario de Veracruz A.C.).* Two liters of artificial seawater (ASW) was prepared by mixing 33 g/L of Ocean Fish salt (PRODAC, Mexico City, Mexico) in ultrapure water (Type 1) (Millipore, Burlington, MA, USA) and sodium hypochlorite (Clorox de Mexico, Estado de Mexico, Mexico). The pH was adjusted to 8.5 using NaOH (Merck, Darmstadt, Germany) and $NaHCO_3$ (Fermont, Nuevo Leon, Mexico). This ASW was poured into a conical container and oxygenated for 1.5 h at 28 °C. Afterward, chlorine was neutralized with two drops of sodium thiosulfate (Clorokill, Biomaa, Estado de Mexico, Mexico). Two hundred milligrams of *A. franciscana* cysts were hydrated in 200 mL of fresh water (Type 1) for 30 min. Then, the cysts were collected using a 50 µm mesh and transferred into ASW for hatching. The system was maintained for 24 h with constant aeration at pH ≅ 8.5, 28 °C, and 1850 lumens of illumination.

Compound preparation

For toxicity assays, a stock solution of 600 mM HO-AAVPA in DMSO (Sigma-Aldrich, Saint Louis, MO, USA) was prepared. From this, a 1 mM HO-AAVPA dilution in ASW was made, resulting in a final DMSO concentration of 0.17%. This solution was sonicated to enhance its solubility. Subsequent serial dilutions were then prepared. A 300 mM sodium valproate (VPA) solution (Sigma-Aldrich, Saint Louis, MO, USA) was prepared in ASW, with DMSO added to a final concentration of 0.17%. Sodium dodecyl sulfate (SDS) (Sigma-Aldrich, Saint Louis, MO 63103, USA) was used as the positive reference (0, 5, 9, 16, 28, and 50 mg/L). HO-AAVPA was synthesized in our workgroup (Prestegui-Matel et al., 2016). Compound concentrations for acute toxicity tests were determined in a preliminary assay using the ArToxkit M method[20], with an initial range-finding test using five concentrations across ten orders of magnitude. All solutions were freshly prepared before each test. The assay was considered valid if the DMSO vehicle control group (ASW + DMSO 0.17%) exhibited viability above 90% and the mortality control (SDS) induced at least 30% mortality in the larvae.

Acute toxicity assay

At the end of the 24-h hatching period, larvae (instar I and II) (Supplementary Data 1, Fig. S1) were collected using a 50 µm mesh. They were transferred to a beaker containing ASW for 2 h. The larvae were concentrated using photo-attraction, then collected with a Pasteur pipette and placed in a 60 mm Petri dish. To minimize dilution during transfer, 500 µL of each test concentration was added to a 24-well plate. Next, sixty larvae were transferred to the 24-well plate, and 9–12 larvae were subsequently transferred to each well of a 96-well plate containing 100 µL of the test compound (HO-AAVPA: 0.1, 0.18, 0.32, 0.56 and 1 mM; VPA: 3, 5.4, 9.6, 16.8, 30, 54, 96, 168 and 300 mM). As negative control groups, *A. franciscana* individuals were treated with ASW and ASW + DMSO 0.17% (vehicle control), respectively. The 96-well plate was sealed with parafilm to prevent evaporation, covered with aluminum foil, and incubated at 25–26.5 °C for 24 h and 48 h. Larvae mortality was recorded at 24 h under a dissecting microscope, with death defined as the absence of movement for 10 s. The plate was re-incubated, and mortality was reassessed at 48 h, with total larvae counts performed after anesthesia with ethanol (Sigma-Aldrich, Saint Louis, MO, USA). Three independent experiments were performed in triplicate using 96-well plates. For each experiment, the number of dead larvae per concentration in 3 wells and the total number of larvae were recorded at 24 h and 48 h of treatment. Corrected mortality percentages relative to vehicle control were calculated using the Schneider-Orelli formula (Eq. 1).

$$Mortality\ (\%) = \frac{\%\,Treatment\ mortality - \%\,Control\ mortality}{100 - \%Control\ mortality} * 100 \quad (1)$$

Lethal concentrations of 50% (LC_{50}) were determined using probit regression curves in R version 4.1.0 (2021-05-18) with the "ecotox" package version 1.4.4[21]. Graphs were generated using the "ggplot2" package version 3.5.1[22].

Teratogenic effect

The teratogenic effect of the compounds was assessed by measuring the length of the larvae. Thirty larvae were incubated in 1 mL of the corresponding compound dilution in 1.5 mL Eppendorf tubes at 25–26.5 °C for 24 h and 48 h. Then, ten larvae were sampled and transferred to a 96-well plate. The larvae were anesthetized with ethanol at a final concentration of 5%, which was increased to 70% for euthanasia. The larvae were then placed on a microscope slide for observation. Microphotographs were taken using an MD35 AmScope camera (AmScope, Irvine, CA, USA), capturing images of at least seven larvae per treatment. The body length of the larvae was measured using AmScope software version 4.11.18573.20210303.

Differences in the mortality percentage and body length were evaluated by a linear mixed-effects model with experiment number as a random effect to account for between-experiment variability. The means of each treatment per drug were then contrasted with the respective time-matched vehicle control group (ASW + DMSO 0.17%). The p-values of the pairwise contrast were adjusted by Dunnett's method.

Metabolomics analysis

Experimental design

The metabolic effects of HO-AAVPA and VPA were evaluated in *A. franciscana* larvae after 24 h and 48 h of exposure using an untargeted metabolomic approach. Approximately 3,000 larvae were incubated in 30 mL of ASW containing the respective compound. Two control groups were established: the first group consisted of individuals incubated in ASW, while the second group served as the vehicle control with a final DMSO concentration of 0.034%. Two sub-lethal concentrations of HO-AAVPA and VPA were used for metabolomic assays[6]. The first was the lethal concentration affecting 10% of the larvae population (LC_{10}) at 24 h, and the second was 20% of the LC_{10}, referred to as LC_1. For HO-AAVPA, the treatments were LC_{10} = 0.2 mM and LC_1 = 0.04 mM, whereas for VPA, the treatments were LC_{10} = 8.95 mM and LC_1 = 1.79 mM. For the preparation of HO-AAVPA and VPA solutions, DMSO was added to achieve a final concentration of 0.034%. The larvae were incubated at 25 °C. After treatment, the larvae were collected by filtration using a 50 µm mesh, flash-frozen in liquid nitrogen, and stored at -80 °C until analysis. One sample per condition and time were collected in seven independent experiments.

Metabolite extraction

The samples were lyophilized and weighed. Before the extraction, 50 µL of internal standards 4-acetamidophenol (Sigma-Aldrich, Saint Louis, MO, USA) at 1200 ppm, carbamazepine (Sigma-Aldrich, Saint Louis, MO, USA) at 700 ppm, glybenclamide (Sigma-Aldrich, Saint Louis, MO, USA) at 400 ppm and diclofenac (Sigma-Aldrich, Saint Louis, MO, USA) at 1200 ppm were added to all samples.

The metabolite extraction followed the procedures described in application note 5991- 3528EN of Agilent Technologies (Agilent Technologies, Santa Clara, CA, USA)[23]. All samples were randomly processed, including two extraction blanks (no sample). For this purpose, 1 mL of pre-chilled − 80 °C methanol (MeOH) (Honeywell International Inc., Morris Plains, NJ, USA) and water (Type I) (2:0.8 v/v) mixture was added to each sample. The samples were sonicated, followed by chloroform (Sigma-Aldrich, Saint Louis, MO, USA) and water addition to obtain a final solvent ratio of 1:2:1.8 ($CHCl_3$:MeOH: H_2O). After vortexing and centrifugation at 4 °C and 5,000 rpm for 30 min, the samples were fractionated into aqueous, protein, and organic phases. The liquid phases and proteins were carefully separated, the organic phase was dried in an orbital incubator (INO-650 M, Prendo, Puebla, Mexico) at 30 °C, and the aqueous phase was dried in a Vacuum Concentrator (Sigma-Aldrich, Saint Louis, MO, USA). The proteins and dried samples were stored at − 80 °C for further analysis.

Metabolomic profiling

The organic fraction of the samples was reconstituted with isopropanol (IPA) (Honeywell International Inc., Morris Plains, NJ, USA) and acetonitrile (ACN) (Honeywell International Inc., Morris Plains, NJ, USA) 90:10 v/v, while the hydrophilic fraction was resuspended in a solution of ACN, methanol, and type I water (ACN: MeOH: H_2O) in a 7:2:1 v/v ratio. The volume of the reconstituted solution was based on the sample weight, and this dilution factor was later used as a normalization factor for each sample. Untargeted metabolomic analysis was performed via liquid chromatography-mass spectrometry (LC-MS/MS) based on standardized methods from Estrada-Pérez et al., 2023[19]. The samples were analyzed in a UHPLC 1290 Infinity II coupled with a Q-TOF with electrospray injection (ESI) (Agilent Technologies, Santa Clara, CA, USA). Polar metabolites were analyzed by hydrophilic interaction liquid chromatography (HILIC), whereas the organic phase was analyzed using reverse-phase (RP) chromatography. Both methods were implemented for positive and negative modes using a nonlinear gradient described in Supplementary Data 1 (Table S1–S4). All samples were analyzed in a single batch. The analysis sequence was randomized to include samples from all treatment groups and time points. To ensure the quality of the analysis, a quality control (QC) sample was prepared by pooling 5 µL of each sample. After system equilibration, solvent blank, IS blank, and extraction blank samples were processed, followed by 5 QC injections. QC was reanalyzed every six samples. The injection for each sample was 2 µL. A total of seven independent samples per treatment and time were analyzed.

Spectral analysis

The LC-MS data were converted to mzML format using Protewizard platform (MsConvert Version: 3.0.23132-2d5b2f2)[24] and then analyzed on the Metaboanalyst 5.0 web-based platform[25], which utilizes the OptiLCMS R package (version 1.0.5) based on an Intel Xeon Processor-based platform[26]. The Best Parameters

algorithm was employed to analyze the raw spectra, which were determined by analyzing five randomly selected QC spectra. The feature table obtained from each method was filtered from blank contaminants and cleaned of isotopes and adducts based on the peak annotations. The stability of data acquisition was demonstrated through PCA analysis, which positioned the QCs at the center of the samples (Supplementary Data 1, Fig. S2).

Data pre-processing and analysis

The data was pre-processed and analyzed using R package version 4.3.2 (2023-10-31 ucrt)[27]. Features that appeared in less than 80% of the samples per class were removed, and samples with more than 51% missing values were excluded. Missing values were then imputed using the K-nearest neighbor algorithm using pmp 1.12.0 packages[28]. Signal correction was performed with the MetaboAnalystR 4.0.0[29] using the EigenMS method[30], considering the sequence order of each sample analysis. Feature abundances were normalized with the sample dilution factor. Features with low inter-sample variability were filtered out using an interquartile range (IQR) filter of 40, while features with high technical variability in QCs were excluded using a 30% RSD threshold.

Significant alterations in the larval metabolome were determined using the Linear functions for extended ANOVA simultaneous component analysis (ALASCA), version 1.0.11[31]. The effect of time was separated from the effect of treatments. This method separates data variability into specific effect matrices representing time and time-treatment interaction. The Jack-knife method (1,000 iterations) was used to validate the model. The features with significant differences compared to vehicle control (ASW + DMSO 0.034%) (FDR < 0.05) were fragmented using the analytical conditions described in the LC-MS analysis.

Putative annotation

The putative annotation of the features was conducted by comparing LC-MS/MS fragmentation spectra to those in the experimental (https://hmdb.ca/downloads, downloaded on 20/Nov/2022) and predicted (downloaded 23/Dec/2022) databases from the HMDB 5.0[32], as well as from the MassBank of North America (MoNA) (https://mona.fiehnlab.ucdavis.edu/downloads downloaded 12/Apr/2024) using the MetaboAnnotation package[33]. The fragmentation spectra were obtained by feature and collision energy using the Spectra package[34] and compared to each database with a tolerance of 10 ppm for the signals and, in the case of MoNA, of the precursor mz[34]. Additionally, the fragmentation spectra were analyzed in the MS-FINDER ver 3.60[35,36] program using a Precursor Oriented Search with Structure finder parameters of Ms2Tolerance = 10 ppm; the spectra were compared with public ("ESI(+) and ESI(-)-MS/MS from standards + bio + in silico", https://systemsomicslab.github.io/compms/msdial/main.html#MSP, last edited on Aug. 8th, 2024), internal experimental (HMDB, SMDPB, and LipidMaps) and in silico libraries. The selection of putative annotations was based on the highest score, considering the minimum value of 0.8 for HMDB and MoNA and 5.0 for MS-Finder. This last value was defined according to the scores obtained by internal standards (Supplementary Data 2).

ChemRICH analysis

We applied the Chemical Similarity Enrichment Analyses (ChemRICH)[37,38] to identify the chemical classes significantly altered with HO-AAVPA and VPA treatments. We consider the subclass chemical taxonomy provided in HMDB v 5.0 (All Metabolites released on 2021-11-17) for chemical clustering. Enrichment p-values were determined using the Kolmogorov–Smirnov test, considering p-values < 0.05 as statistically significant.

Pathway analysis

We evaluated the impact on metabolic pathways by performing Pathway Analysis in Metaboanalyst 6.0[39] with the Kyoto Encyclopedia of Genes and Genomes (KEGG) ID[40–43] of putative metabolites with FDR < 0.05 as the input list. We selected the *Daphnia pulex* KEGG library[40–43] as the reference map for the analysis. We used a hypergeometric test for over-representation method and relative betweenness centrality for topological analysis to assess node importance.

Results

Determination of LC_{50} in *A. franciscana* larvae

In the acute toxicity assay, HO-AAVPA and VPA showed toxic effects within 24 h of treatment, resulting in 100% lethality of the larvae at their highest concentrations (Table 1). Based on the results, it is evident that HO-AAVPA exhibits higher toxic effects than VPA, with LC_{50} = 0.45 mM (106.23 mg/L) and 41.1 mM, respectively (Table 2 and Supplementary Data 1, Fig. S3). The toxic effect becomes more pronounced at 48 h, both compounds decreased their LC_{50} values (HO-AAVPA = 0.32 mM vs. VPA = 18.70 mM). The difference in potency between HO-AAVPA and VPA corresponds to 2 orders of magnitude, suggesting that 100 times higher concentrations of VPA are required to achieve the same lethal effect.

Teratogenic effects of HO-AAVPA and VPA in *A. franciscana* larvae

The teratogenic effects of HO-AAVPA and VPA were evaluated at 24 and 48 h of treatment using larvae length as a morphological indicator. As illustrated in Fig. S4 of the Supplementary data 1, both control groups (ASW and ASW + DMSO 0.17%) demonstrated statistically significant growth. Table 3 resumes the effect on the body length of HO-AAVPA and VPA treatments. The results showed that HO-AAVPA is lower teratogenic than VPA (Fig. 1). The concentrations of HO-AAVPA that affect the development of larvae are higher than its LC_{50}. In contrast, larvae treated with 9.6 mM VPA showed statistically significant differences in body length, which slightly exceeds the LC_{10} of 8.95mM.

The impact of HO-AAVPA and VPA on the metabolome was evaluated by exposing larvae to sub-lethal concentrations (LC_1 and LC_{10}) for 24 and 48 h. Principal component analysis (PCA) showed that time was the main factor causing changes among larvae, with the samples from each hour being separated along the

Drug	Concentration		Mortality %	
	mg/L	mM	24 h	48 h
Control (ASW)	0	0	4.97 ± 0.99[a]	8.85 ± 2.97[a]
DMSO (ASW + DMSO 0.17%)	0	0	4.44 ± 2.22[a]	5.56 ± 2.94[a]
HO-AAVPA	23.53	0.10	2.38 ± 2.38	7.76 ± 4.67
	42.36	0.18	1.03 ± 1.15	16.96 ± 6.69
	75.31	0.32	10.41 ± 5.92	30.34 ± 15.25
	131.78	0.56	60.16 ± 18.53***	77.3 ± 13.49***
	235.33	1.00	97.81 ± 1.1***	100 ± 0***
VPA	499	3	1.19 ± 3.15	7.06 ± 3.61
	897	5.4	1.83 ± 3.66	4.98 ± 4.86
	1595	9.6	10.08 ± 8.85	26.43 ± 8.52
	2792	16.8	11.11 ± 11.85	29.41 ± 11.96
	4986	30	35.05 ± 12.82	62.42 ± 14.69***
	8974	54	37.32 ± 15.84*	82.22 ± 9.04***
	15,954	96	70.18 ± 14.77***	96.35 ± 2.13***
	27,920	168	98.85 ± 1.15***	100 ± 0***
	49,857	300	100 ± 0***	100 ± 0***

Table 1. Mortality percentage in *Artemia franciscana* larvae. % Mortality: Corrected mortality percentage calculated by Schneider-Orelli's formula was reported as mean ± SEM, with DMSO 0.17% serving as the control group for correction. [a] Raw value of the mortality percentage. Asterisks denote statistically significant differences compared to the respective time-matched DMSO 0.17% group (***$p < 0.001$, Dunnett adjusted p-values).

Drug	Time (h)	LC	Concentration	LCL	UCL
			mM (mg/L)		
HO-AAVPA	24	10	0.20 (47.4)	0.08	0.29
		50	0.45 (106.23)	0.32	0.67
	48	10	0.13 (29.49)	0.06	0.18
		50	0.32 (75.75)	0.24	0.43
VPA	24	10	8.95 (1487.01)	4.80	13.41
		50	41.10 (2509.7)	30.32	56.56
	48	10	4.71 (783.1)	3.01	6.49
		50	18.70 (1257.06)	14.94	23.21

Table 2. Lethal concentrations of HO-AAVPA and VPA in *Artemia franciscana* larvae. *LC* lethal concentration, *LCL* lower control limit 95%, *UCL* upper control limit 95%.

first principal component (PC) in each LC-MS method (Supplementary Data 1, Fig. S2). At the same time, PC2 mainly explains the treatment effect. In addition, samples in vehicle control groups (ASW + DMSO 0.034%) closely resembled untreated individuals (ASW control group), indicating that it is a suitable control for subsequent analyses.

The data were analyzed using the ALASCA method to evaluate the impact of the treatments[31]. The influence of time on the metabolome is consistent across all treatments, with parallel trends but different score values (Supplementary Data 1, Fig. S5). After separating the effect of time, it was observed that HO-AAVPA generally affects the *A. franciscana* metabolome differently compared to VPA (Supplementary Data 1, Fig. S6). Supplementary Data 3 shows the feature loads for each PC.

Putative metabolites deregulated in HO-AAVPA and VPA treatments

The putative identity of the significant deregulated features (Supplementary Data 4) was determined by spectral similitude comparison. The complete list can be consulted in Supplementary Data 5. Figure 2 highlights the top 50 metabolites with the most significant changes among all treatments. L-serine and isobutyryl-L-carnitine were the metabolites that increase by VPA. In the same way, L-glutamine, L-asparagine, and the pyridones dihydrothymine and dihydrouracil showed moderate increases with VPA.

In contrast, HO-AAVPA did not produce any significant impact on the above metabolites, but it raised the abundance of the sesquiterpenoid mintsulfide and the steroids 3beta,7alpha-Dihydroxy-5-cholestenoate and 4alpha-Carboxy-5alpha-cholesta-8-en-3beta-ol, among others. The most notable change induced by HO-AAVPA was the downregulation of the pheromone 7E,9E,11-Dodecatrienyl acetate.

Drug	Concentration		Body length	
	mg/L	mM	24 h	48 h
DMSO (ASW + DMSO 0.17%)	0	0	0.77 ± 0.01	0.83 ± 0.01
HO-AAVPA	23.53	0.10	0.79 ± 0.011	0.82 ± 0.014
	42.36	0.18	0.77 ± 0.007	0.78 ± 0.015
	75.31	0.32	0.76 ± 0.01	0.83 ± 0.011
	131.78	0.56	0.7 ± 0.014	0.69 ± 0.022***
	235.33	1.00	0.66 ± 0.018***	0.58 ± 0.018***
VPA	499	3	0.78 ± 0.008	0.8 ± 0.01
	897	5.4	0.74 ± 0.012	0.77 ± 0.012
	1595	9.6	0.69 ± 0.011***	0.68 ± 0.021***
	2792	16.8	0.67 ± 0.009***	0.66 ± 0.017***
	4986	30	0.67 ± 0.008***	0.64 ± 0.013***
	8974	54	0.61 ± 0.015***	0.57 ± 0.017***
	15,954	96	0.56 ± 0.011***	0.54 ± 0.01***
	27,920	168	0.52 ± 0.014***	0.5 ± 0.011***
	49,857	300	0.51 ± 0.009***	0.5 ± 0.01***

Table 3. Body length o f*Artemia franciscana*. Body length is reported as mean ± SEM of at least 29 individuals per condition, evaluated in three independent experiments. Data were analyzed using a linear mixed effects model. Asterisks indicate statistically significant differences compared to the respective time-matched DMSO vehicle control group (***$p < 0.001$, Dunnett adjusted p-values).

In the same way, the abundance of some triacylglycerides (TG) was downregulated with both concentrations of HO-AAVPA. However, this effect is only present at 24 h (Supplementary Data 1, Fig. S7). The p-values and log2FC are detailed in (Supplementary Data 4).

Metabolic set enrichment analysis by chemical similarity

To gain a deeper understanding of the biological effects caused by VPA and HO-AAVPA on larvae metabolism, we conducted a ChemRICH analysis[38]. This analysis is centered on the chemical ontology of deregulated metabolites, which offers a comprehensive view of metabolic changes within chemical clusters. This approach proves particularly valuable for understanding the biological impact of treatments in an organism with an undefined metabolic map, such as *A. franciscana*.

The results of the ChemRICH analysis (Supplementary Data 6) show that HO-AAVPA had a major impact on lipid metabolites (Fig. 3a). At 24 h, both LC_1 and LC_{10} treatments caused significant changes in triacylglycerides (triradylcglycerols) metabolites, with opposing effects: LC_1 decreased the abundance of the metabolites in this cluster, but increased LC_{10}, like linoleic acids and derivatives. The treatment with HO-AAVPA at 48 h using both concentrations substantially affected the metabolism of glycerophosphocholines and glycerophosphoethanolamines, resulting in mixed changes among the metabolites of this subclass.

VPA also increases lipid abundance, especially in larvae treated with LC_1 for 48 h, affecting several subclasses of glycerophospholipids and linoleic acid and derivatives (Fig. 3b). Interestingly, VPA LC_{10} downregulates the abundance of the metabolites in ceramide and glycerophosphoinositol clusters, with this decrease sustained up to 48 h.

The lowest VPA concentration treatment positively impacts most C2-C6 acylcarnitines (fatty acid esters cluster), while LC_{10} affects short and long-chain acylcarnitines. However, over the 48-h treatment period, only the increase in isobutyryl-L-carnitine abundance remains constant at both concentrations, whereas most acylcarnitines re-establish their levels or decrease. Similarly, HO-AAVPA treatments significantly alter these metabolites, although most remain unchanged. Unlike VPA, malonyl carnitine is the metabolite with the most sustained alterations in HO-AAVPA treatment (Supplementary Data 1, Fig. S8). The impact of VPA on the abundance of amino acids and their derivatives is significant, showing an upward trend in most of the metabolites of this cluster (Supplementary Data 1, Fig. S9-S10).

Enrichment pathway analysis

The effect of HO-AAVPA and VPA on metabolic pathways was assessed through an enrichment pathway analysis, taking the *Daphnia pulex* metabolic map as a reference (Fig. 4). The results depict glycerophospholipid and sphingolipid metabolism as the major deregulated pathways under HO-AAVPA treatment (LC_{10} at 48 h) (Supplementary Data 1, Table S5). VPA also impacts these pathways similarly to HO-AAVPA treatment (Supplementary Data 1, Table S6).

On the other hand, the most notable effect of VPA treatment is the great impact on alanine, aspartate, and glutamate metabolism.

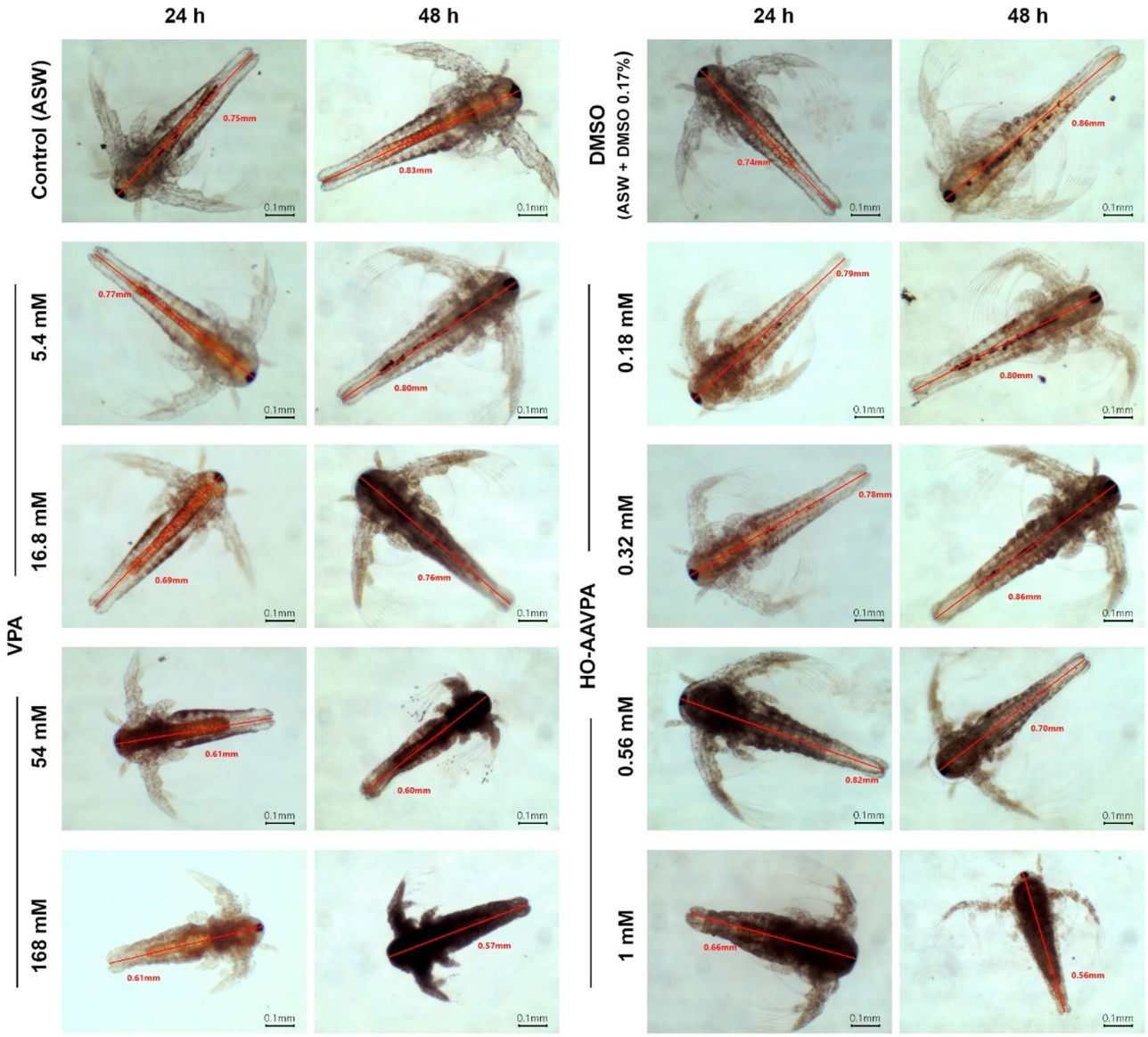

Fig. 1. Microphotographs of *A. franciscana* metanauplii (instar II+) in control groups (ASW and ASW + DMSO 0.17%) and treated with VPA and HO-AAVPA for 24 and 48 h. Red lines indicate the body length from the eye to the end of the tail.

Discussion

This study evaluated the toxic and teratogenic effects of HO-AAVPA and VPA in *A. franciscana*, a cost-effective in vivo model commonly employed for screening the cytotoxic potential of new compounds. Our proposal aimed to enhance the application of this model through untargeted metabolomics, providing a deeper biochemical characterization of the effects and the modes of action of these compounds.

Our findings are consistent with previous studies in cancer cell cultures, as they not only demonstrate the toxic capacity of HO-AAVPA in this organism, but also that its effect is more potent than VPA[15,19]. Interestingly, we also found that the LC_{50} of HO-AAVPA in larvae is comparable to the IC_{50} reported in the MCF-7 cell line (476.1 µM)[19].

Lestari et al. (2017)[10] reported the toxicity of VPA in *A. salina*, resulting in 100% lethality at 2500 mg/L (15 mM). Our study found that this effect was achieved above 96 mM at 48 h (Table 1). Despite the differences in concentrations, both results suggest VPA has a weaker toxicity ($LC_{50} > 1000$ mg/L)[44].

VPA is less toxic than HO-AAVPA, but with a stronger teratogenic capacity in this crustacean. These results align with those presented by Cristóbal-Luna et al. (2020)[18], reporting a lower frequency and severity of alterations in the embryonic development of CD1 mice with HO-AAVPA (600 mg/kg) compared to VPA (500 mg/kg).

HDAC inhibitors, especially pan-inhibitors which are hydroxamic acid derivatives, are known for their teratogenic effects[45,46]. The morphological alterations induced by VPA and its derivatives are linked to their

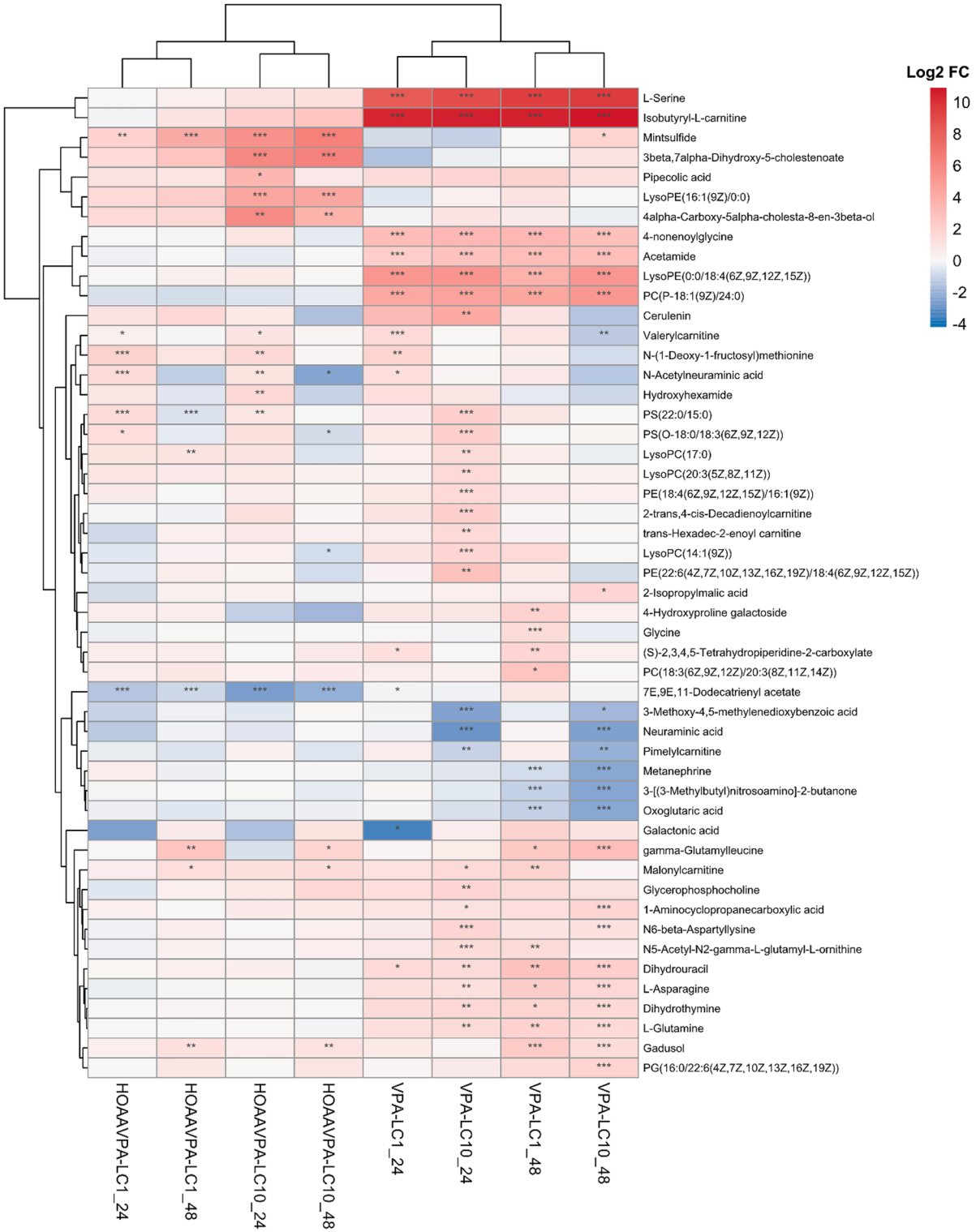

Fig. 2. Heat map of the top 50 putative metabolites deregulated by HO-AAVPA and VPA treatments. The heatmap shows the log2 Fold change values calculated from the feature abundance mean under each condition from seven independent biological samples, compared to the vehicle control group (ASW + DMSO 0.034%). The clusters were performed using Euclidean distance. Asterisks represent FDR adjusted $*p < 0.05$, $**p < 0.01$, $***p < 0.001$.

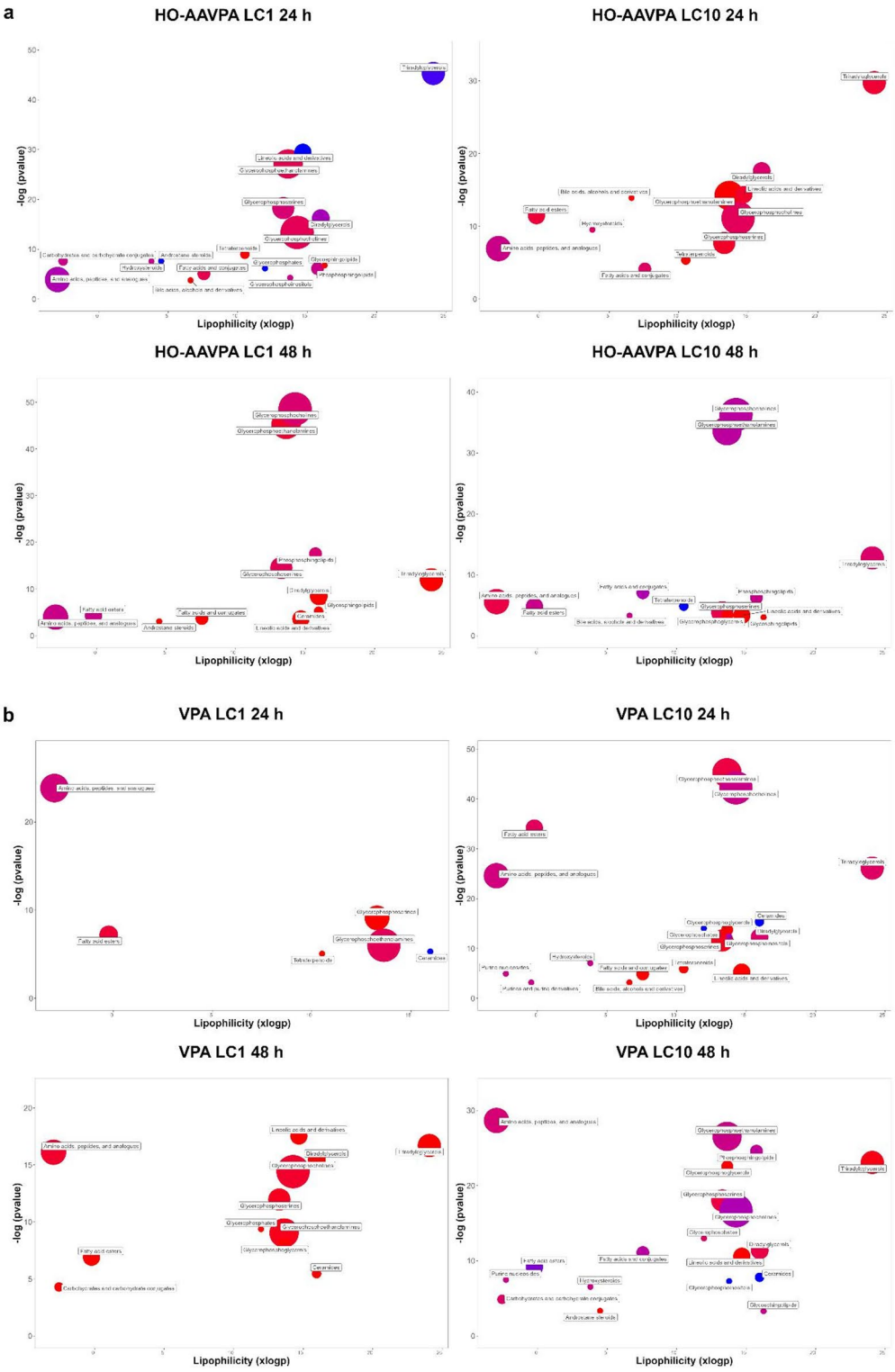

Fig. 3. ChemRICH analysis of putative metabolites altered by (**a**) HO-AAVPA and (**b**) VPA treatments. Plots show the clusters of significantly altered metabolites according to chemical subclass. Enrichment p-values were determined by the Kolmogorov–Smirnov test. The node sizes represent the total number of metabolites in each cluster, and the node color indicates the proportion of increase (red), decrease (blue), or mixed changes (purple) in metabolites compared to larvae treated with the vehicle control (ASW + DMSO 0.034%). The clusters are distributed on the Y-axis according to the statistical significance of the changes, while on the X-axis, they appear according to their lipophilicity.

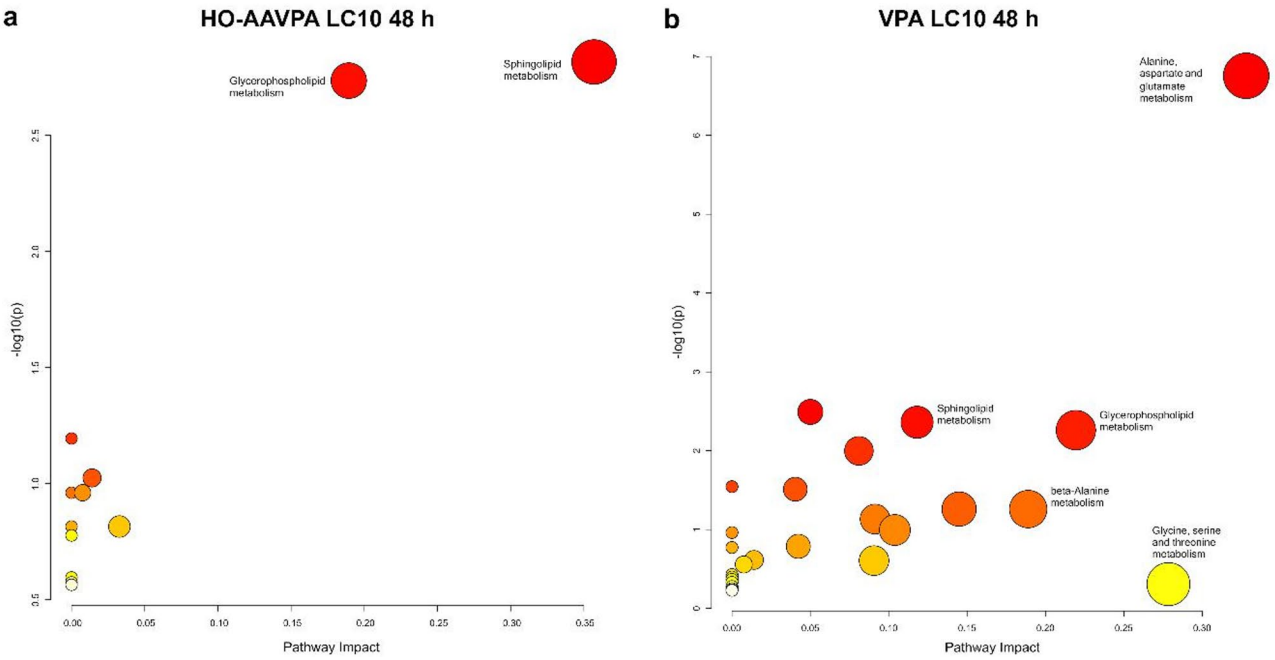

Fig. 4. Pathway enrichment analysis. Plots show the major metabolic pathways impacted by (**A**) HO-AAVPA and (**B**) VPA LC_{10} at 48 h on A. franciscana larvae. The circle size denotes the magnitude of pathway impact, and the color indicates the significance of the impact on each pathway.

structure, HDAC inhibitory properties[47], and are hardly associated with its phase 1 metabolism by CYP450. However, the carboxyl modification has been associated with lower teratogenic activity[47,48]. Interestingly, the hydroxy-benzamide bond on VPA yield the in HO-AAVPA changes the structure of VPA, making it a zinc-binding group with improved HDAC selectivity and its metabolism result in a di-hydroxylate compound with better anti-proliferative properties[49]. Also, tucidinostat, a benzamide that belongs to the non-hydroxamic class HDACi, has a hydroxy-benzamyde bond that is comparable to HO-AAVPA[50].

Treatment of larvae with sublethal concentrations of HO-AAVPA and VPA altered the abundance of lipid-like molecules, impacting the sphingolipid and glycerophospholipids metabolic pathways. These findings align with those previously reported by Estrada-Pérez et al. (2023)[19], who point out that HO-AAVPA and VPA treatment induced the deregulation of these pathways in MCF-7 And MDA-MB-231 breast cancer cell lines.

The treatment with HO-AAVPA LC_{10} increased certain oxysterols, such as 3beta,7alpha-dihydroxy-5-cholestenoate, 3b-hydroxy-5-cholenoic acid, 7-ketodeoxycholic acid, and 4alpha-carboxy-5alpha-cholesta-8-en-3beta-ol. These molecules are potentially related to oxidative stress[51,52]. Future studies should explore whether HO-AAVPA employs lipid peroxidation as part of its toxic mechanism of action.

VPA treatment also affected the abundance of acylcarnitines. In this sense, in vitro[53] and pediatric patient studies[54,55] have reported the impact of VPA on acylcarnitine metabolism. This includes elevated levels of 3-hydroxybutyrylcarnitine[54,55], hexanoylcarnitine, and octanoylcarnitine[55], and reduced levels of acetylcarnitine[53]. Changes in acylcarnitine metabolism have been associated with the hepatotoxic effects of VPA. The accumulation of acyl carnitines in the liver can disrupt fatty acid metabolism by inhibiting mitochondrial β-oxidation[56].

Given that naupliar stages represent the active life form of *A. franciscana* and are metabolically the most active, modifications of lipid metabolic pathways and deregulation of bioactive lipids directly impact crucial stages of the brine shrimp life cycle[57].

Regarding alterations in amino acids and derivates, alanine, aspartate, and glutamate metabolism was the pathway most significantly affected by VPA treatment. Our results are consistent with the findings reported by Zhou et al., (2020)[58], who showed this effect in the MDA-MB-231 cells. These metabolic changes have also been observed in other organisms with VPA treatment. In KM mice, VPA administration changes pathways associated with amino acids, fatty acids, and energy metabolism in a tissue-specific manner, with the kidney showing the most significant effects[59]. In this study, the metabolites that exhibited the most significant increase in several tissues included L-phenylalanine, L-threonine, L-proline, L-5-Oxoproline, L-alanine, L-glutamic acid, and serine, determined by GC-MS chromatography to assess the levels of these metabolites.

It has been proposed that alterations in these metabolic pathways are part of the mechanism of VPA-induced toxicity, particularly in the liver[60]. Although treatment with HO-AAVPA also shares alterations in similar pathways and even with the same trend in some amino acids (Supplementary Data1, Fig. S9-S10), the impact is of different magnitude[19]. This could explain the differences in toxicity previously reported between these two compounds in different models and organisms[17,18], as well as their difference in pharmacological potency[19].

Our findings are based on the identification of metabolites with confidence level 2, and their confirmation depends on comparison with reference standards. Nevertheless, it is worth mentioning that gadusol, a metabolite previously reported in *A. franciscana*[8], was also putatively identified in our study. Furthermore, our analysis found a feature at 138.0525 mz using the HILIC-P method. This feature was tentatively identified as trigonelline in the HMDB, MoNA, and MS-FINDER databases. Trigonelline has been previously found in other marine species, such as *Hydractinia echinata*[61] and the coral *Dendronephthya* sp[62]. ; however, it has not been reported in *A. franciscana*. Although trigonelline was the top match in the three databases, there were other coincident metabolites, including 4-aminobenzoic acid, methyl nicotinate, and homarine, the latter reported in both *A. franciscana*[8] and *H. echinata*[61]. 7E,9E,11-Dodecatrienyl acetate was the most deregulated metabolite by HO-AAHPA treatment. This metabolite has only been reported in the insect *Lobesia botrana*. Although pheromones have not been identified in *A. franciscana*, Tapia et al., (2015)[63] suggested the presence of sexual semiochemicals that regulate courtship behavior in this crustacean. Furthermore, other members of the Branchiopoda class, such as *Daphnia pulex*, produce other chemical signals that play a role in inter-species communication[64].

It is important to note that the results of this study were obtained from hatched individuals from non-decapsulated cysts, and the experiments were conducted under non-sterile conditions. Consequently, interactions with microorganisms were present and may have influenced the response to treatments. To reduce the complexity of interactions and to confirm the mechanisms of action of these molecules, it is advisable to evaluate the toxic activity of compounds under gnotobiotic conditions[65]. Nevertheless, non-gnotobiotic conditions better represent the natural ecosystem and interactions with commensal microorganisms.

Our findings are consistent with other studies conducted under sterile conditions[19,53,58], as well as in vivo[18,59], and clinical investigations[54,55]. This consistency underscores the validity of our results despite the non-sterile environment in which our experiments were performed.

Despite the limitations of the invertebrate animal model[66], the brine shrimp has proven its worth by capturing the main metabolic effects induced by HO-AAVPA and VPA previously reported[19,53,58]. This supports the use of *A. franciscana* as a valid preclinical model for characterizing the biological action of new molecules and their mode of action through metabolomics studies, in addition to its applications in toxicity assays of environmental contaminants[67–70]. However, it is urgent to increase research on this organism to establish a metabolome database and construct its metabolic pathway. Moreover, integrating other omics techniques, such as proteomics, would provide a more comprehensive characterization of new compounds, significantly enhancing the capacity of this model.

Conclusion

The acute toxicity assays in *A. franciscana* larvae confirm that HO-AAVPA has higher toxicity effects than VPA, which agrees with its cytotoxic effects in breast cancer cells previously reported. However, HO-AAVPA has lower teratogenic effects than VPA based on *A. franciscana* larvae morphological changes that agree with other results reported in a rat model. In addition, our research confirms metabolic alterations in lipid and amino acid metabolism as the main targets of HO-AAVPA and VPA treatment in *A. franciscana* larvae, respectively. Most significantly, these findings suggest changes in metabolic pathways which depict the mode of action of these compounds across different organisms. Therefore, this work proposes integrating the *Artemia franciscana* as an alternative model for toxicological characterization of new compounds. This could not only reduce the use of mammals in research, thereby addressing ethical concerns, but also significantly accelerate the discovery and development of new drugs.

Data availability

The datasets generated and/or analysed during the current study are available in the Zenodo repository, https://doi.org/10.5281/zenodo.13984579.

Received: 19 December 2024; Accepted: 20 May 2025
Published online: 28 May 2025

References

1. Singh, V. K. & Seed, T. M. How necessary are animal models for modern drug discovery? *Expert Opin. Drug Discov.* **16**, 1391–1397 (2021).
2. Alves-Pimenta, S., Colaço, B., Oliveira, P. A. & Venâncio, C. Development features on the selection of animal models for teratogenic testing. in Teratogenicity Testing: Methods and Protocols (ed Félix, L.) 67–104 (Springer US, New York, NY, (2024).
3. Libralato, G., Prato, E., Migliore, L., Cicero, A. M. & Manfra, L. A review of toxicity testing protocols and endpoints with *Artemia* spp. *Ecol. Indic.* **69**, 35–49 (2016).
4. Filipe, M. S. et al. Lethality bioassay using *Artemia salina L.*. *J. Vis. Exp. JoVE* e64472 https://doi.org/10.3791/64472 (2022).
5. Ntungwe, N. Artemia species: an important tool to screen general toxicity samples. *Curr. Pharm. Des.* **26**, 2892–2908 (2020).
6. Gong, Y. et al. Molecular mechanisms of zooplanktonic toxicity in the Okadaic acid-producing dinoflagellate *Prorocentrum lima*. *Environ. Pollut.* **279**, 116942 (2021).
7. Morgan, M. A., Griffith, C. M., Volz, D. C. & Larive, C. K. TDCIPP exposure affects *Artemia franciscana* growth and osmoregulation. *Sci. Total Environ.* **694**, 133486 (2019).
8. Morgan, M. A. et al. Evaluating sub-lethal stress from Roundup® exposure in Artemia franciscana using 1H NMR and GC-MS. *Aquat. Toxicol. Amst Neth.* **212**, 77–87 (2019).
9. Kerster, H. W. & Schaeffer, D. J. Brine shrimp (Artemia salina) nauplii as a teratogen test system. *Ecotoxicol. Environ. Saf.* **7**, 342–349 (1983).
10. Lestari, M. W., Soemardji, A. A., Fidrianny, I. & Yusuf, A. T. The capability of Brine shrimp test as a teratogenicity screening system. *Asian J. Pharm. Clin. Res.* **10**, 454 (2017).

11. Álvarez-Alarcón, N., Osorio-Méndez, J. J., Ayala-Fajardo, A., Garzón-Méndez, W. F. & Garavito-Aguilar, Z. V. Zebrafish and Artemia salina in vivo evaluation of the recreational 25 C-NBOMe drug demonstrates its high toxicity. *Toxicol. Rep.* **8**, 315–323 (2021).
12. Lu, Y., Yu, J. A. & Well-Established Method for the Rapid Assessment of Toxicity Using *Artemia* spp. Model. In *Assessment and Management of Radioactive and Electronic Wastes* (ed. El-Din Saleh, H.) https://doi.org/10.5772/intechopen.85730 (IntechOpen, 2020).
13. Pang, H. & Hu, Z. Metabolomics in drug research and development: the recent advances in technologies and applications. *Acta Pharm. Sin B.* **13**, 3238–3251 (2023).
14. Fragoso-Vázquez, M. J. et al. UHPLC-MS/MS studies and antiproliferative effects in breast Cancer cells of Mexican Sargassum. *Anticancer Agents Med. Chem.* **23**, 76–86 (2023).
15. Prestegui-Martel, B. et al. N-(2-hydroxyphenyl)-2-propylpentanamide, a valproic acid Aryl derivative designed in Silico with improved anti-proliferative activity in HeLa, rhabdomyosarcoma and breast cancer cells. *J. Enzyme Inhib. Med. Chem.* **31**, 140–149 (2016).
16. Correa-Basurto, A. M. et al. Pharmacokinetics and tissue distribution of *N*-(2-hydroxyphenyl)-2-propylpentanamide in Wistar rats and its binding properties to human serum albumin. *J. Pharm. Biomed. Anal.* **162**, 130–139 (2019).
17. Correa Basurto, A. M. et al. Hepatotoxic evaluation of N-(2-Hydroxyphenyl)-2-Propylpentanamide: A novel derivative of valproic acid for the treatment of Cancer. *Molecules* **28**, 6282 (2023).
18. Cristóbal-Luna, J. M., Correa-Basurto, J., Mendoza-Figueroa, H. L. & Chamorro-Cevallos, G. Anti-epileptic activity, toxicity and teratogenicity in CD1 mice of a novel valproic acid arylamide derivative, *N*-(2-hydroxyphenyl)-2-propylpentanamide. *Toxicol. Appl. Pharmacol.* **399**, 115033 (2020).
19. Estrada-Pérez, A. R. et al. Untargeted LC-MS/MS metabolomics study of HO-AAVPA and VPA on breast Cancer cell lines. *Int. J. Mol. Sci.* **24**, 14543 (2023).
20. Microbiotests, I. ARTOXKIT M. Artemia toxicity screening test for estuarine and marine waters. https://www.microbiotests.com/wp-content/uploads/2019/07/artemia-toxicity-test_artoxkit-m_standard-operating-procedure.pdf (2019).
21. Hlina, B. L., Birceanu, O., Robinson, C. S., Dhiyebi, H. & Wilkie, M. P. The relationship between thermal physiology and lampricide sensitivity in larval sea lamprey (*Petromyzon marinus*)☆. *J. Gt Lakes Res.* **47**, S272–S284 (2021).
22. Wickham, H. et al. ggplot2: Create elegant data visualisations using the grammar of graphics. (2024).
23. Blackwell, A., Aja, S., Zhou, W., Graham, D. & Ronnett, G. V. Multi-omics compatible protocols for Preparation and extraction of biological samples for wide coverage in untargeted metabolomics experiments. https://www.agilent.com/cs/library/technicaloverviews/public/5991-3528EN.pdf (2013).
24. Chambers, M. C. et al. A cross-platform toolkit for mass spectrometry and proteomics. *Nat. Biotechnol.* **30**, 918–920 (2012).
25. Pang, Z. et al. MetaboAnalyst 5.0: narrowing the gap between Raw spectra and functional insights. *Nucleic Acids Res.* **49**, W388–W396 (2021).
26. Pang, Z., Chong, J., Li, S. & Xia, J. MetaboAnalystR 3.0: toward an optimized workflow for global metabolomics. *Metabolites* **10**, 186 (2020).
27. R Core Team. *R: A Language and Environment for Statistical Computing* (R Foundation for Statistical Computing, 2023).
28. Jankevics, A., Lloyd, G. R. & Weber, R. J. M. pmp: Peak matrix processing and signal batch correction for metabolomics datasets. https://doi.org/10.18129/B9.bioc.pmp (2023).
29. Pang, Z. et al. MetaboAnalystR 4.0: a unified LC-MS workflow for global metabolomics. *Nat. Commun.* **15**, 3675 (2024).
30. Karpievitch, Y. V., Nikolic, S. B., Wilson, R., Sharman, J. E. & Edwards, L. M. Metabolomics data normalization with eigenms. *PLOS ONE.* **9**, e116221 (2014).
31. Jarmund, A. H., Madssen, T. S. & Giskeødegård, G. F. ALASCA: an R package for longitudinal and cross-sectional analysis of multivariate data by ASCA-based methods. *Front Mol. Biosci.* **9**, (2022).
32. Wishart, D. S. et al. HMDB 5.0: the human metabolome database for 2022. *Nucleic Acids Res.* **50**, D622–D631 (2022).
33. Rainer, J. et al. A modular and expandable ecosystem for metabolomics data annotation in R. *Metabolites* **12**, 173 (2022).
34. Gatto, L., Rainer, J., Gibb, S. & Spectra spectra infrastructure for mass spectrometry data. https://doi.org/10.18129/B9.bioc.Spectra (2023).
35. Lai, Z. et al. Identifying metabolites by integrating metabolome databases with mass spectrometry cheminformatics. *Nat. Methods* **15**, 53–56 (2018).
36. Tsugawa, H. et al. Hydrogen rearrangement rules: computational MS/MS fragmentation and structure Elucidation using MS-FINDER software. *Anal. Chem.* **88**, 7946–7958 (2016).
37. Barupal, D. K., Fan, S. & Fiehn, O. Integrating bioinformatics approaches for a comprehensive interpretation of metabolomics datasets. *Curr. Opin. Biotechnol.* **54**, 1–9 (2018).
38. Barupal, D. K. & Fiehn, O. Chemical similarity enrichment analysis (ChemRICH) as alternative to biochemical pathway mapping for metabolomic datasets. *Sci. Rep.* **7**, 14567 (2017).
39. Pang, Z. et al. MetaboAnalyst 6.0: towards a unified platform for metabolomics data processing, analysis and interpretation. *Nucleic Acids Res.* **52**, W398–W406 (2024).
40. Kanehisa, M., Furumichi, M., Sato, Y., Kawashima, M. & Ishiguro-Watanabe M. KEGG for taxonomy-based analysis of pathways and genomes. *Nucleic Acids Res.* **51**, D587–D592 (2023).
41. Kanehisa, M., Furumichi, M., Sato, Y., Matsuura, Y. & Ishiguro-Watanabe, M. KEGG: biological systems database as a model of the real world. *Nucleic Acids Res.* **53**, D672–D677 (2025).
42. Kanehisa, M. Toward Understanding the origin and evolution of cellular organisms. *Protein Sci.* **28**, 1947–1951 (2019).
43. Kanehisa, M. & Goto, S. K. E. G. G. Kyoto encyclopedia of genes and genomes. *Nucleic Acids Res.* **28**, 27–30 (2000).
44. Meyer, B. N. et al. Brine shrimp: a convenient general bioassay for active plant constituents. *Planta Med.* **45**, 31–34 (1982).
45. Giavini, E. & Menegola, E. Teratogenic activity of HDAC inhibitors. *Curr. Pharm. Des.* **20**, 5438–5442 (2014).
46. Liang, T. et al. Targeting histone deacetylases for cancer therapy: trends and challenges. *Acta Pharm. Sin B.* **13**, 2425–2463 (2023).
47. Eikel, D., Lampen, A. & Nau, H. Teratogenic effects mediated by Inhibition of histone deacetylases: evidence from quantitative structure activity relationships of 20 valproic acid derivatives. *Chem. Res. Toxicol.* **19**, 272–278 (2006).
48. Chang, X. et al. Quantitative in vitro to in vivo extrapolation for developmental toxicity potency of valproic acid analogues. *Birth Defects Res.* **114**, 1037–1055 (2022).
49. Galindo-Alvarez, N. L., Mendoza-Figueroa, H. L., Rosales-Hernández, M. C., Bakalara, N. & Correa-Basurto, J. Decrease in cell viability of breast cancer cells by a di-hydroxylated derivative of *N*-(2-hydroxyphenyl)-2-propylpentanamide. http://www.eurekaselect.com
50. Sixto-López, Y. et al. N-(2′-Hydroxyphenyl)-2-Propylpentanamide (HO-AAVPA) inhibits HDAC1 and increases the translocation of HMGB1 levels in human cervical cancer cells. *Int. J. Mol. Sci.* **21**, 5873 (2020).
51. Björkhem, I., Diczfalusy, U. & Oxysterols *Arterioscler. Thromb. Vasc Biol.* **22**, 734–742 (2002).
52. Mahalakshmi, K. et al. Chapter 44 - Neurotoxicity induced by lipid metabolism–associated endogenous toxicants. In *Natural Molecules in Neuroprotection and Neurotoxicity* (ed. Oliveira, M. R. de) 1083–1104 https://doi.org/10.1016/B978-0-443-23763-8.00079-8 (Academic Press, 2024).
53. Silva, M. F. B., Jakobs, C., Duran, M., de Almeida, I. T. & Wanders, R. J. A. Valproate induces *in vitro* accumulation of long-chain fatty acylcarnitines. *Mol. Genet. Metab.* **73**, 358–361 (2001).

54. Nakajima, Y. et al. Evaluation of valproate effects on acylcarnitine in epileptic children by LC–MS/MS. *Brain Dev.* **33**, 816–823 (2011).
55. Werner, T. et al. Effects of valproate on acylcarnitines in children with epilepsy using ESI-MS/MS. *Epilepsia* **48**, 72–76 (2007).
56. Ma, Y. et al. The serum acylcarnitines profile in epileptic children treated with valproic acid and the protective roles of peroxisome proliferator-activated receptor a activation in valproic acid-induced liver injury. *Front. Pharmacol.* **13**, 1048728 (2022).
57. Lopalco, P., Lobasso, S., Lopes-dos-Santos, R. M. A., Van Stappen, G. & Corcelli, A. Lipid profile changes during the development of Artemia franciscana, from cysts to the first two naupliar stages. *Front. Physiol.* **9**, (2019).
58. Zhou, X. et al. Metabolomics reveals the effect of valproic acid on MCF-7 and MDA-MB-231 cells. *Xenobiotica* **50**, 252–260 (2020).
59. Gao, Y. et al. Comprehensive analysis of metabolic changes in male mice exposed to sodium valproate based on GC-MS analysis. *Drug Des. Devel Ther.* **16**, 1915–1930 (2023).
60. Ezhilarasan, D. & Mani, U. Valproic acid induced liver injury: an insight into molecular toxicological mechanism. *Environ. Toxicol. Pharmacol.* **95**, 103967 (2022).
61. Berking, S. Homarine (N-methylpicolinic acid) and trigonelline (N-methylnicotinic acid) appear to be involved in pattern control in a marine hydroid. *Development* **99**, 211–220 (1987).
62. Kawamata, M., Kon-ya, K. & Miki, W. Trigonelline, an antifouling substance isolated from an octocoral dendronephthya Sp. *Fish. Sci.* **60**, 485–486 (1994).
63. Tapia, C. et al. Courtship behavior and potential indications for chemical communication in Artemia franciscana (Kellog 1906). *Gayana Concepc.* **79**, 152–160 (2015).
64. Yasumoto, K., Nishigami, A., Kasai, F., Kusumi, T. & Ooi, T. Isolation and absolute configuration determination of aliphatic sulfates as the Daphnia Kairomones inducing morphological defense of a phytoplankton. **54**, (2006).
65. Do, M. A. et al. Silver nanoparticle toxicity on Artemia parthenogenetica nauplii hatched on axenic tryptic soy agar solid medium. *Sci. Rep.* **13**, 6365 (2023).
66. Ségalat, L. Invertebrate animal models of diseases as screening tools in drug discovery. *ACS Chem. Biol.* **2**, 231–236 (2007).
67. Ekonomou, G. et al. Mortality and effect on growth of Artemia franciscana exposed to two common organic pollutants. *Water* **11**, 1614 (2019).
68. Kamalakannan, M., Rajendran, D., Thomas, J. & Chandrasekaran, N. Synergistic impact of nanoplastics and nanopesticides on Artemia salina and toxicity analysis. *Nanoscale Adv.* **6**, 3119–3134 (2024).
69. Philibert, D. A., Parkerton, T., Marteinson, S. & de Jourdan, B. Calibration of an acute toxicity model for the marine crustacean, *Artemia franciscana*, nauplii to support oil spill effect assessments. *Sci. Total Environ.* **866**, 161270 (2023).
70. Sultan, M. et al. Comparative toxicity of polystyrene, polypropylene, and polyethylene nanoplastics on Artemia franciscana Nauplii: a multidimensional assessment. *Environ. Sci. Nano* **11**, 1070–1084 (2024).

Acknowledgements

We want to express our gratitude to the Procuraduría Estatal de Protección al Medio Ambiente- Aquarium del Puerto de Veracruz, and especially to Biologist Guadalupe Campos Bautista of the Live Food Laboratory for their technical advice in standardizing the hatching method of Artemia franciscana. We also thank Dr. Olga Hernández of the Universidad Autónoma de la Ciudad de México (UACM) for her assistance in sample drying. CFP acknowledges the support provided by CONAHCYT under the program "Estancias Posdoctorales por México" 2021–2022.

Author contributions

Conceptualization: JCB, CFP. Methodology: CFP, AREP. Investigation: HLMF, CFP. Data curation, Formal analysis, Project administration, Validation, Visualization, and Writing—original draft: CFP. Resources and Writing—review and editing: HLMF, JBGV, MCRH, JCB. Funding acquisition and Supervision: JCB.

Funding

This research was funded by the National Council of Humanities, Sciences and Technologies (CONAHCYT) and Instituto Politécnico Nacional (IPN) by its Secretaría de Investigación y Posgrado under the project SIP20240517.

Declarations

Competing interests

The authors declare no competing interests.

Ethical approval

This protocol was approved by the biosecurity committee from Escuela Superior de Medicina of IPN under the register number ESM-CBS-03/19-01-2023. Although the research involved an unregulated invertebrate species, all experimental procedures adhered to ethical standards established by the committee.

Additional information

Supplementary Information The online version contains supplementary material available at https://doi.org/10.1038/s41598-025-03325-9.

Correspondence and requests for materials should be addressed to C.F.-P. or J.C.-B.